

# A feasible approach to all-electronic digital labeling and readout for cell identification†

D. K. Wood,<sup>a</sup> G. B. Braun,<sup>b</sup> J.-L. Fraikin,<sup>a</sup> L. J. Swenson,<sup>a</sup> N. O. Reich<sup>b</sup> and A. N. Cleland\*<sup>a</sup>

Received 10th November 2006, Accepted 7th February 2007

First published as an Advance Article on the web 1st March 2007

DOI: 10.1039/b616442k

We present two critical innovations that enable a unique, purely electronic approach to microfluidic whole-cell analysis, focusing on the problem of cell identification and sorting. We used fully-scalable lithographic techniques to microfabricate digital barcodes, providing a means for low-cost, large volume production. We have demonstrated molecular functionalization of the barcodes, using biotin–streptavidin, as well as human CD4 antibody, and we have successfully linked the barcodes to polystyrene beads using the biotin–streptavidin complex. This functionalization allows unique barcodes to be attached to specific cell types, based on phenotype. We have also implemented an electronic barcode readout scheme, using a radio frequency microsensors integrated in an elastomeric microfluidic channel, that can read individual barcodes at rates in excess of 1000 labels  $s^{-1}$ . The barcodes are biologically compatible, and coupled with the electronic sensing technology, provide a route to compact, inexpensive, disposable cell identification, sorting and purification.

## 1. Introduction

The high-throughput identification, sorting and purification of individual biological cells from a complex cell population is a common problem in biology and medicine. In particular, multiplexed cell sorting has applications to immunology,<sup>1,2</sup> cancer detection<sup>3</sup> and stem-cell based therapeutic medicine.<sup>4</sup> High-throughput multiplexed whole cell analysis, if implemented in a low-cost, portable system, could serve as an analytic tool for blood analysis at the clinical level, serving to detect rare bacterial infections or blood-borne cancer cells, the latter possibly an indicator of metastatic cancer growth. Such systems could also serve as a tool for harvesting hematopoietic stem cells from adult populations, or from cord blood. The potential, highly appealing use of stem cells for tissue regeneration will also likely rely on high-throughput screening, in order to separate different classes of differentiated stem cells from one another, a procedure that will likely utilize surface protein expression.<sup>5</sup> Multiplexed sorting schemes have also found important applications in the separation and purification of biological molecules for drug screening and drug discovery.<sup>6</sup>

The sorting of cells and molecules is typically achieved using optical labeling and sensing, typified by fluorescence-activated cell sorters (FACS).<sup>7</sup> In optically-based labeling, fluorophores are attached either to proteins expressed on the cell surface or those expressed in the intracellular volume. Labeled cells are then passed through an optical analysis system,

where the fluorescent signal is used to sort and quantify the cell population. Optical multiplexing schemes have been developed,<sup>2,8–13</sup> allowing labeling of diverse cell populations, with a practical, commercially-available limit of order ten distinct fluorophores, allowing sorting of about ten distinct cell types. In general, however, these optically-based labeling techniques involve relatively bulky and expensive optical components to excite, detect, and analyze the fluorescence signals. This limits the number of parallel readout channels available at reasonable cost and physical instrument size, even when microfluidic systems are used for the sorting procedure.<sup>14–17</sup> Other separation techniques, including dielectrophoretic (DEP)<sup>18,19</sup> and magnetic<sup>20</sup> sorting have been investigated, but most of these methods either still require optical detection, or are passive, with no active detection and discrimination mechanism.

All-electronic sensing, as distinct from optically-based techniques, provides a much more compact, scalable approach, easily combined with microfluidic lab-on-a-chip systems, and eliminating the need for costly and expensive optical components. Very inexpensive hand-held systems can quite conceivably be implemented using such non-optical methods. There is, however, a lack of basic bioanalytic tools that can offer equal or superior performance in an electronic rather than an optical format. Several electronic detection methods have been explored, but these methods have been severely limited in throughput and in their ability to sort multiple cell types.<sup>21,22</sup> Here we present two important tools in this area, describing a method for the digital labeling of individual cells with digital electronic bar-coded labels, and demonstrating a sensing technique that allows very high speed readout of these labels, precluding the need for optical instrumentation. The labeling and readout capabilities provide the basic functionality needed for a miniature, all-electronic cell sorter.

<sup>a</sup>Department of Physics, University of California at Santa Barbara, Santa Barbara, CA, 93106, USA

<sup>b</sup>Department of Chemistry and Biochemistry, University of California at Santa Barbara, Santa Barbara, CA, 93106, USA

† The HTML version of this article has been enhanced with colour images.

## 2. Experimental

### 2.1. Barcode design and fabrication

The electronic barcodes are designed to present a position-dependent response when passed over a reader that is sensitive to changes in the local radio frequency impedance. The barcodes are fabricated by embedding patterned metal stripes in a micron-scale bar of photodefineable epoxy (SU-8 2000, MicroChem Corp., Newton, MA). This cross-linked epoxy serves as a stable structural material, robust to most biologically-relevant chemical processes.<sup>23,24</sup> In addition, the epoxy can be functionalized for hybridization with biomolecules or cells,<sup>25,26</sup> making it a good material for cell labeling. The metal stripes, which generate the coded electronic signal, are entirely embedded in the epoxy, so that metal biocompatibility issues are circumvented. We have explored the use of both gold and aluminium stripes, the latter favored for its excellent electrical conductivity as well as low mass density. The barcode structures demonstrated here comprise a 100 nm thick patterned aluminium layer sealed between two 100 nm thick layers of epoxy (Fig. 1(a)), and have overall dimensions of  $100 \times 20 \times 0.3 \mu\text{m}^3$ , comparable to optical barcode labels (see *e.g.* ref. 12). This makes the labels roughly ten times longer than the cells they will label, which is perhaps somewhat cumbersome, although we are not aware that this presents any significant constraints. The lithographic patterning technology allows the lateral dimensions of the labels to be further reduced by a factor of 50 to 100, making sub-micron labels quite feasible. Readout of much smaller labels however presents more of a challenge, as discussed below.

We used a silicon wafer as a handle for label fabrication, first coating the silicon with a sacrificial layer of germanium. The photodefineable epoxy was spun-cast to the desired thickness, and patterned using conventional photolithography. The metal layer was deposited and patterned on top of the epoxy using a standard lift-off process, and the second layer of epoxy patterned on top of the metal. Curing of the second epoxy layer permanently bonds the two epoxy layers together. An image of an array of barcodes prior to release is shown in Fig. 1(b). The silicon handle with the patterned devices was then placed into stock hydrogen peroxide to dissolve the germanium, releasing the barcodes into solution. The peroxide solution was replaced with a saline–sucrose working solution prior to the measurement.

Each of the barcode labels described here includes 10 patterned metal encoding elements (bits), where a metal stripe encodes a “1” and a gap between stripes encodes a “0”. This design allows dual-use readout, using either an electronic or an optical detector. By monitoring the transmitted or reflected light in a standard optical sensing setup, the opaque (reflective) 1’s and the transparent 0’s can be differentiated. Optical readout, in both reflection and transmission, is shown for a single barcode in Fig. 1(c).

### 2.2. Biological functionalization

We have demonstrated biochemical functionalization of the barcode labels with biotin–streptavidin, successfully linked CD4 antibody to the barcodes as a molecular recognition label

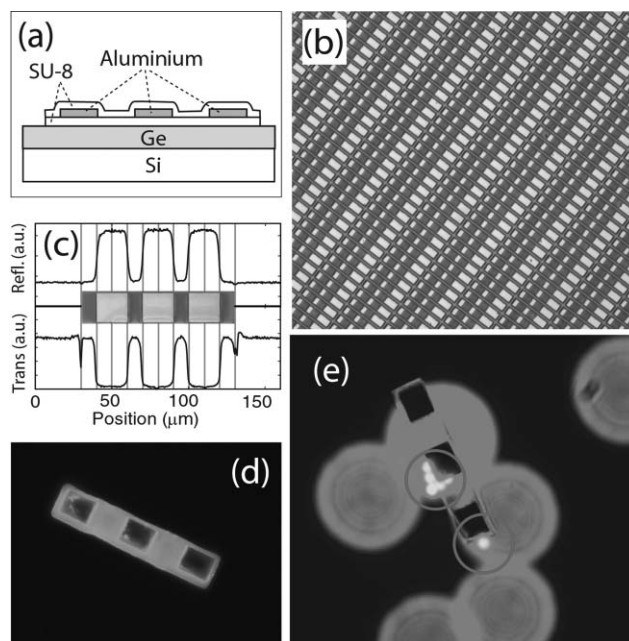


**Fig. 1** Lithographically patterned barcodes with surface functionalization. (a) Cross section of barcode structure prior to release. Aluminium stripes are sandwiched between layers of SU-8, supported by a sacrificial Ge layer on a Si handle. (b) Array of microfabricated barcodes prior to release from substrate. Each barcode is  $100 \mu\text{m}$  in length. Prior to release, the exposed side of the barcodes is functionalized with biotin. After release, the other side is passivated with tris(hydroxymethyl) aminomethane. (c) Optical readout (reflection and transmission) of a single barcode, showing readout capability in an optical platform. (d) Streptavidin-functionalized barcodes were exposed to biotin-modified primary antibody and then Alexa Fluor 488<sup>®</sup>-modified secondary antibody. Image indicates positive binding of primary antibody, and specific binding of secondary antibody, through green Alexa fluorescence. (e) Barcodes with streptavidin-modified,  $6 \mu\text{m}$ -diameter polystyrene beads adhering to the biotinylated side, indicating positive biotin–streptavidin linkages. Bound beads are indicated by the two circles; large diffuse discs are from beads outside the focal plane.

for human T-cells expressing the CD4 protein, and shown that the streptavidin–biotin complex can successfully bind the barcodes to polystyrene beads. Prior to releasing the barcodes from the silicon handle, they were amine-treated and then coated with biotin. After release into saline, Cy3-modified streptavidin (Invitrogen, Carlsbad CA) was added to the mixture. Biotinylation and subsequent streptavidin binding was verified by observing the yellow fluorescence of the bound Cy3-modified streptavidin. We then treated the streptavidin-modified bars with a biotin-modified, anti-human CD4 antibody (mouse IgG1  $\kappa$ ; eBioscience, San Diego CA). To verify binding of this antibody, the bars were treated with an Alexa Fluor 488<sup>®</sup>-modified secondary antibody (goat anti-mouse IgG (H + L); Invitrogen, Carlsbad CA), which specifically binds to the anti-human CD4 primary antibody. A control, which was treated with the secondary antibody but not the primary, showed no Alexa Fluor 488<sup>®</sup> fluorescence, but still tested positive for the presence of Cy3-streptavidin. Using this technique, the barcodes can be used to recognize human T-cells expressing the CD4 protein, which serves as the target

for the human immunodeficiency virus (HIV). As a preliminary step to binding mammalian cells, binding of barcode labels to polystyrene beads has also been demonstrated, using the biotin–streptavidin complex. Streptavidin-modified, 6  $\mu\text{m}$ -diameter polystyrene beads (Polysciences, Inc., Warrington, PA) were mixed with biotinylated barcodes in  $1 \times$  phosphate buffered saline (PBS) solution, successfully binding beads to labels, as shown in Fig. 1(e). These results demonstrate the ability of these barcodes to specifically label cells, using cell surface epitopes. We have had preliminary success in binding labels to mammalian cells, in addition to labeling beads, and are performing more work on verifying binding specificity using control experiments.

### 2.3. Device operation

We implemented electronic readout of the barcodes using a high-bandwidth radio frequency (rf) microsensor embedded in a microfluidic channel, a version of which we have demonstrated previously as a high-throughput Coulter counter.<sup>27</sup> The sensor detects changes in the local electrical impedance, due to the presence of particles or labels suspended in a saline solution flowing through the microfluidic channel. Electrolytic interfacial impedances, which limit the sensitivity and bandwidth of low-frequency electronic sensors in similar solutions, become negligible at frequencies above  $\sim 10$  MHz. The active detection region of the sensor comprises two 10  $\mu\text{m}$ -wide coplanar gold electrodes, with a separation of 10  $\mu\text{m}$ , embedded in a microfluidic channel with cross-sectional dimension of  $100 \times 50 \mu\text{m}^2$ . The microchannels were molded in poly(dimethyl siloxane) (PDMS) elastomer,<sup>28</sup> and mounted on glass substrates with pre-patterned detection electrodes. The circuit and device schematic are shown in Fig. 2(a) and

2(b). The inductive matching network, forming a resonant tank circuit with the device and solution capacitance, allows high sensitivity by matching the source to the solution impedance.<sup>27,29</sup> When properly impedance-matched, or “tuned,” the measurement is dark-field, giving maximum sensitivity to small impedance changes. Fig. 2(c) shows the reflected power as a function of frequency for two different solutions. With a tuned reflectance below  $-70$  dB, achieved here with  $1 \times$  PBS, the source is well-matched to the working solution, corresponding to a radio frequency reflectance of less than 1 part in 10 million. Equivalent tuning can be achieved for a wide range of salt concentrations. In our measurements, we operated the device near 40 MHz, with a usable bandwidth of 6.8 MHz, and typically excited the device with a  $-35$  dBm ( $4 \text{ mV}_{\text{rms}}$ ) signal. The reflected power from the device is amplified using two series amplifiers (AM1431, Miteq, Hauppauge, NY), each with 36 dB of gain and a noise temperature of  $\sim 100$  K. The signal is then sent to a radio frequency lock-in amplifier (SR844, Stanford Research Systems, Palo Alto, CA), which is phase-locked to the primary signal, and the mixed-down signal amplitude recorded using a 100 MHz digital oscilloscope.

### 2.4. Barcode readout

The barcodes present a position-dependent impedance as they pass in single file over the microsensor electrodes. The saline solution is mildly conducting, so the insulating epoxy 0's increase the net electrical resistance, while the metal 1's are highly conducting and decrease the resistance. As a label passes over the detector, the alternating 0's and 1's change the local impedance, modulating the reflected rf power. In Fig. 2(d) we sketch the reflected power as a function of the resistance

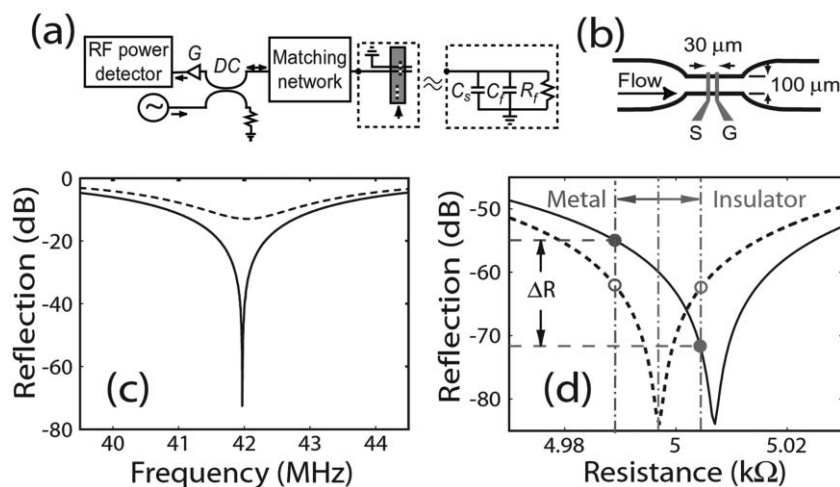


**Fig. 2** Electronic detection scheme. (a) Circuit schematic; G is a low-noise amplifier and DC a directional coupler. Impedance matching (“tuning”) is achieved using a matching network. The microfluidic channel is shown schematically in the left dashed box, and its lumped circuit representation in the right dashed box. (b) Schematic of microfluidic channel and metal electrode sensor, with relevant dimensions. “S” and “G” represent the signal and ground electrodes, respectively. (c) Radio frequency reflectance for two different solutions in microfluidic channel. Solid curve:  $1 \times$  PBS with  $0.45 \text{ g mL}^{-1}$  sucrose; dashed curve: deionized water, with sensor tuned to  $1 \times$  PBS. (d) Simulated reflected power as a function of inter-electrode resistance. Dash-dot central vertical line indicates solution resistance, dash-dot left vertical line is solution plus metal stripe resistance, dash-dot right vertical line is solution plus insulator resistance. When the circuit is tuned to solution (dashed curve), a metal (left open circle) and insulating stripe (right open circle) give roughly the same change in reflected power, yielding poor differentiation. When the circuit is tuned to higher resistance (solid curve), a metal (filled left circle) and insulating stripe (filled right circle) give a large reflectance difference  $\Delta R$ .

between the device electrodes, for fixed tuning. When optimally tuned (solid curve), the reflected power is at a minimum, so that any impedance change increases the reflected power. While this yields high sensitivity to changes in impedance, it does not give high contrast between the conducting and insulating barcode stripes. By tuning the circuit to a slightly higher impedance (Fig. 2(d)), the insulating 0's decrease, while the metal 1's increase, the reflected power, achieving high contrast. The orientation of the barcodes is also important. Viscous drag aligns the bars along their long axis, so they preferentially pass over the sensor in the proper orientation; front-to-back orientation is not controlled, which could be problematic, but can be made irrelevant by using mirror-symmetric stripe encoding, or by indicating orientation using a fixed coding element.

### 3. Results and conclusions

In Fig. 3 we display time-domain rf reflectance of the sensor for eight distinct barcode labels flowing at  $\bar{v}_{\text{fluid}} = 11 \text{ mm s}^{-1}$ . Each label gives a strong signal with a clearly distinguishable pattern. The biggest variations in signal amplitude and rate are due to bars passing over the sensor at different heights in the microchannel, where the Poiseuille parabolic flow pattern gives a height-dependent velocity.

We have implemented a prototype recognition scheme to demonstrate the ability to identify bar encodings from the reflection signal. We display the outcome of this analysis using three distinct bar patterns, those in Fig. 3(f), (g) and (h). These patterns were chosen to demonstrate the ability to distinguish differing stripe counts as well as differing stripe patterns. Bar-to-bar variations in signal amplitude and signal rate were eliminated by scaling both reflection strength, and extremal peak distance in time, to uniform values for all traces. The analysis used a two-dimensional differentiation, the first analytic based on the number of peaks in the reflection signal, a number that is directly correlated with the number of metal encoding stripes. Peaks were detected as  $3\sigma$  variations in signal from the baseline noise. The second analytic was based on assigning an error score to each (unknown) label when compared to a template signal, each template generated by one (known) label. The error score was calculated as the summed absolute difference of the unknown trace from the

template. Representative signal traces from bars with patterns “0110000110” and “0110011110” are compared with the template “0110000110” in Fig. 4(a). Traces similar to the template result in small error scores, while dissimilar traces yield large error scores. Fig. 4(b) shows the mean error scores for a population of labels with the patterns “1100110011”, “0110000110”, and “0110011110” compared against the three templates for the same encodings. For each label, the correct template has the lowest score, with a  $2\sigma$  exclusion for the other templates. The two-dimensional analysis results, comprising peak number and error scores for each label, using the templates “0110000110” and “0110011110”, are shown in Fig. 4(c) and (d), respectively. While admittedly representing a small population of labels, labels differing in stripe number are clearly perfectly distinguishable, and the label error scoring provides a reasonable second discriminant. The main source of error in the scoring analysis is that the time scaling is not consistent, as no “start” or “stop” markers were included in the encoding. Adding such markers to the ends of the bars will minimize this variation, and presumably make the error scores a much more robust discriminant. In addition, such markers would allow discrimination of asymmetric label patterns.

To demonstrate the high throughput capability of the readout scheme, we flowed bars at ten times the flow rate ( $\bar{v}_{\text{fluid}} = 110 \text{ mm s}^{-1}$ ), shown in Fig. 5(a) and (b), corresponding to a readout rate of more than 1000 labels per second. The fidelity of the pattern is clearly retained, and higher readout speeds are easily attainable.

This labeling and readout system has applications to the identification and sorting of diverse cell populations. We have demonstrated the preliminary steps for cell identification, which would be achieved by functionalizing the barcodes with affinity labels, designed to bind specifically to epitopes expressed on certain cell types' surfaces.<sup>19</sup> The specific binding would thus be electronically encoded, and would provide the basis for sorting and purification using a downstream microfluidic sorter.<sup>19,30,31</sup> The barcode fabrication process is simple and intrinsically scalable, both in the size and number of labels produced. Here we have encoded 10 distinct bits, yielding in principle  $2^{10} = 1024$  distinguishable barcode labels. By reducing the bit width by a factor of two,  $2^{20}$  or more than a million distinct patterns could be encoded. The electronic readout we employ offers several distinct advantages over

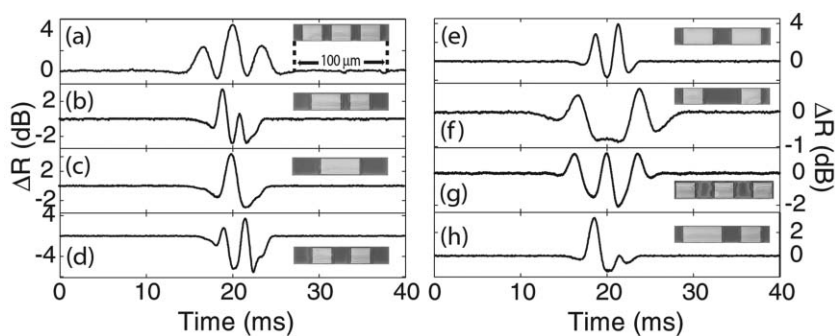


**Fig. 3** Bar code readout. Reflectance change  $\Delta R$  due to barcode labels flowing at  $\bar{v}_{\text{fluid}} = 11 \text{ mm s}^{-1}$ : (a) “0110110110”, (b) “0011101100”, (c) “0001111000”, (d) “0011001100”, (e) “0111001110”, (f) “0110000110”, (g) “1100110011” and (h) “0111100110”. Peaks represent metal, while dips are epoxy. Insets are optical micrographs of actual barcodes, where yellow is metal.

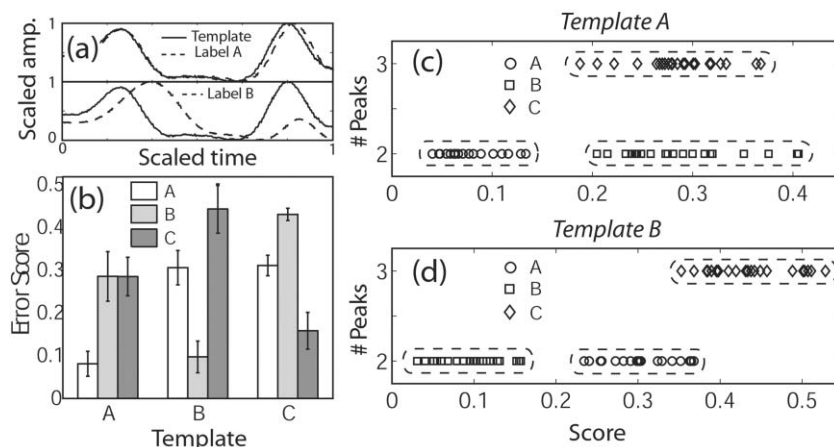


**Fig. 4** Pattern comparison and recognition. The letters A, B and C correspond to the patterns “0110000110”, “0110011110” and “1100110011”, respectively. (a) Comparison of scaled signal between the template for A and representative labels A (upper panel) and B (lower panel). The solid line represents the template; the dashed line is compared to the label. (b) Mean label comparison score for patterns A, B, and C compared to templates of the same patterns. Error bars represent standard deviation from the mean score. Analyzed number of peaks vs. label comparison score for individual labels compared to templates (c) A and (d) B. Dotted outlines indicate distinct labels separable through this analysis.

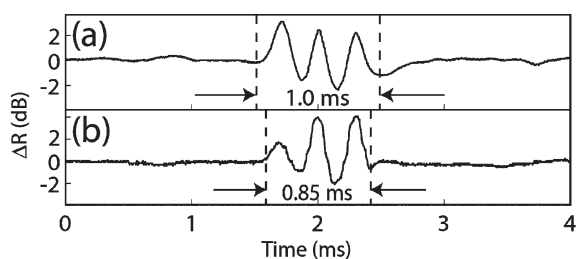


**Fig. 5** High throughput detection. High throughput readout demonstrated by reflectance changes  $\Delta R$  measured for barcodes “1100110011” and “0110110110” flowing at  $v_{\text{fluid}} = 110 \text{ mm s}^{-1}$ .

optical techniques: Facile and inexpensive fabrication, micron-scale dimensions, easy scalability to large numbers of parallel channels, and straightforward readout electronics. We believe a relatively straightforward reduction of the sensor and bar size scales could achieve roughly 1 micron dimensions. This approach, in summary, offers the potential for a truly portable, disposable, and inexpensive all-electronic bio-analysis platform.

## Acknowledgements

This work was supported in part by the Army Research Office through the UCSB Institute for Collaborative Biotechnologies under contract DAAD19-03-D-0004, and the DMEA/DARPA Center for Nanoscience Innovation for Defense. We would like to thank Omair Sadaat and Frank Cleary for assistance in fabrication, Ben Youngblood for sample preparation, and Bob Hill and Siddharth Rajan for processing assistance.

## References

- 1 S. C. De Rosa, L. A. Herzenberg, L. A. Herzenberg and M. Roederer, *Nat. Med.*, 2001, **7**(2), 245–248.
- 2 S. C. De Rosa, J. M. Brechley and M. Roederer, *Nat. Med.*, 2003, **9**(1), 112–117.
- 3 R. T. Krivacic, A. Ladanyi, D. N. Curry, H. B. Hsieh, P. Kuhn, D. E. Bergsrud, J. F. Kepros, T. Barbera, M. Y. Ho, L. B. Chen, R. A. Lerner and R. H. Bruce, *Proc. Natl. Acad. Sci. U. S. A.*, 2004, **101**(29), 10501–10504.
- 4 R. L. Rietze, H. Valcanis, G. F. Brooker, T. Thomas, A. K. Voss and P. F. Bartlett, *Nature*, 2001, **412**(6848), 736–739.
- 5 Q. Gan, T. Yoshida, O. G. McDonald and G. K. Owens, *Stem Cells*, 2007, **25**, 2–9.
- 6 K. Braeckmans, S. C. De Smedt, M. Leblans, R. Pauwels and J. Demeester, *Nat. Rev. Drug Discovery*, 2002, **1**(6), 447–456.
- 7 S. F. Ibrahim and G. van den Engh, *Curr. Opin. Biotechnol.*, 2003, **14**(1), 5–12.
- 8 W. C. Chan and S. Nie, *Science*, 1998, **281**(5385), 2016–2018.
- 9 S. R. Nicewarner-Pena, R. G. Freeman, B. D. Reiss, L. He, D. J. Pena, I. D. Walton, R. Cromer, C. D. Keating and M. J. Natan, *Science*, 2001, **294**(5540), 137–141.
- 10 H. Fenniri, L. Ding, A. Ribbe and Y. Zyrianov, *J. Am. Chem. Soc.*, 2001, **123**(33), 8151–8152.
- 11 M. Han, X. Gao, J. Z. Su and S. Nie, *Nat. Biotechnol.*, 2001, **19**(7), 631–635.
- 12 M. J. Dejneka, A. Streltsov, S. Pal, A. G. Frutos, C. L. Powell, K. Yost, P. K. Yuen, U. Muller and J. Lahiri, *Proc. Natl. Acad. Sci. U. S. A.*, 2003, **100**(2), 389–393.
- 13 P. K. Yuen, M. Despa, C.-C. J. Li and M. J. Dejneka, *Lab Chip*, 2003, **3**(3), 198–201.
- 14 A. Y. Fu, C. Spence, A. Scherer, F. H. Arnold and S. R. Quake, *Nat. Biotechnol.*, 1999, **17**(11), 1109–1111.
- 15 A. Wolff, I. R. Perch-Nielsen, U. D. Larsen, P. Friis, G. Goranovic, C. R. Poulsen, J. P. Kutter and P. Telleman, *Lab Chip*, 2003, **3**(1), 22–27.
- 16 A. Revzin, K. Sekine, A. Sin, R. G. Tompkins and M. Toner, *Lab Chip*, 2005, **5**(1), 30–37.
- 17 M. Eisenstein, *Nature*, 2006, **441**(7097), 1179–1185.
- 18 A. B. Fuchs, A. Romani, D. Freida, G. Medoro, M. Abonnenc, L. Altomare, I. Chartier, D. Guergour, C. Villiers, P. N. Marche, M. Tartagni, R. Guerrieri, F. Chatelain and N. Maresi, *Lab Chip*, 2006, **6**(1), 121–126.
- 19 X. Y. Hu, P. H. Bessette, J. R. Qian, C. D. Meinhardt, P. S. Daugherty and H. T. Soh, *Proc. Natl. Acad. Sci. U. S. A.*, 2005, **102**(44), 15757–15761.
- 20 N. Pamme and C. Wilhelm, *Lab Chip*, 2006, **6**(8), 974–980.
- 21 L. L. Sohn, O. A. Saleh, G. R. Facer, A. J. Beavis, R. S. Allan and D. A. Nottelman, *Proc. Natl. Acad. Sci. U. S. A.*, 2000, **97**(20), 10687–10690.
- 22 S. Gawad, K. Cheung, U. Seger, A. Bertsch and P. Renaud, *Lab Chip*, 2004, **4**, 241–251.
- 23 H. Lorenz, M. Despont, N. Fahrni, J. Brugger, P. Vettiger and P. Renaud, *Sens. Actuators, A: Physical*, 1998, **64**(1), 33–39.
- 24 V. Seidemann, S. Butefisch and S. Buttgenbach, *Sens. Actuators, A: Physical*, 2002, **97–98**, 457–461.

- 25 R. Marie, S. Schmid, A. Johansson, L. Ejsing, M. Nordstrom, D. Haflliger, C. B. Christensen, A. Boisen and M. Dufva, *Biosens. Bioelectron.*, 2006, **21**(7), 1327–1332.
- 26 M. Calleja, J. Tamayo, M. Nordstrom and A. Boisen, *Appl. Phys. Lett.*, 2006, **88**(11), 113901.
- 27 D. K. Wood, S.-H. Oh, S.-H. Lee, H. T. Soh and A. N. Cleland, *Appl. Phys. Lett.*, 2005, **87**(18), 184106.

- 28 Y. Xia, E. Kim, X.-M. Zhao, J. A. Rogers, M. Prentiss and G. M. Whitesides, *Science*, 1996, **273**(5273), 347–349.
- 29 R. J. Schoelkopf, P. Wahlgren, A. A. Kozhevnikov, P. Delsing and D. E. Prober, *Science*, 1998, **280**(5367), 1238–1242.
- 30 P. Dittrich and P. Schwill, *Anal. Chem.*, 2003, **75**(21), 5767–5774.
- 31 M. Dürr, J. Kentsch, T. Müller, T. Schnelle and M. Stelzle, *Electrophoresis*, 2003, **24**, 722–731.

## Textbooks from the RSC

The RSC publishes a wide selection of textbooks for chemical science students. From the bestselling *Crime Scene to Court*, 2nd edition to groundbreaking books such as *Nanochemistry: A Chemical Approach to Nanomaterials*, to primers on individual topics from our successful *Tutorial Chemistry Texts series*, we can cater for all of your study needs.

Find out more at [www.rsc.org/books](http://www.rsc.org/books)

Lecturers can request inspection copies – please contact [sales@rsc.org](mailto:sales@rsc.org) for further information.



07040692

Registered Charity No. 207890

RSC Publishing

[www.rsc.org/books](http://www.rsc.org/books)